MNRAS **000**, 1–13 (2015) Preprint 22 July 2016 Compiled using MNRAS LATEX style file v3.0

A new method for testing isotropy with Shannon entropy

Biswajit Pandey★
Department of Physics, Visva-Bharati University, Santiniketan, Birbhum, 731235, India

arXiv:1512.03562v2 [astro-ph.CO] 21 Jul 2016

22 July 2016

ABSTRACT

We propose a method for testing isotropy of a three-dimensional distribution using Shannon entropy. We test the method on some Monte Carlo simulations of isotropic and anisotropic distributions and find that the method can effectively identify and characterize different types of hemispherical asymmetry inputted in a distribution. We generate anisotropic distributions by introducing pockets of different densities inside homogeneous and isotropic distributions and find that the proposed method can effectively quantify the degree of anisotropy and determine the geometry of the pockets introduced. We also consider spherically symmetric radially inhomogeneous distributions which are anisotropic at all points other than the centre and find that such anisotropy can be easily characterized by our method. We use a semi analytic galaxy catalogue from the Millennium simulation to study the anisotropies induced by the redshift space distortions and find that the method can separate such anisotropies from a general one. The method may be also suitably adapted for any two dimensional maps on the celestial sphere to study the hemispherical asymmetry in other cosmological observations.

Key words: methods: numerical - galaxies: statistics - cosmology: theory - large scale structure of the Universe.

1 INTRODUCTION

The Cosmological principle which assumes that the Universe is statistically homogeneous and isotropic on sufficiently large scales is one of the fundamental assumptions of modern cosmology. This assumption can not be proved in a rigorously mathematical sense but can be verified from various cosmological observations. Testing the assumption of statistical homogeneity and isotropy is important as our interpretations of various cosmological observations are based on our current understanding of the Universe which in turn relies on the cosmological principle. Homogeneity and isotropy are two different but related aspects which may or may not coexist in a system. The Universe can be homogeneous without being isotropic or can be isotropic around a point without being homogeneous. But isotropy around each and every point guarantees homogeneity.

Observationally the most powerful evidence for isotropy is provided by the the near uniform temperature of the Cosmic Microwave Background Radiation (CMBR) across the whole sky (Penzias & Wilson 1965; Smoot et al. 1992; Fixsen et al. 1996). However the CMBR is not completely isotropic. Over the years many studies have reported power asymmetries and unlikely alignments of low multipoles (Schwarz et al. 2004; Land & Magueijo 2005; Hanson & Lewis 2009; Moss et al. 2011; Gruppuso et al. 2013; Dai et al. 2013). The asymmetries found in WMAP were largely attributed to deficiencies in the foreground subtraction (Bennett et al. 2011) and non circularity of beams (Das et al. 2014). However recent analysis of PLANCK data by Planck Collaboration et al. (2014) reported that the power asymmetry persist on scales corresponding to $l \sim 600$ and the deviations from isotropy are at high statistical significance ($3-\sigma$). A further analysis using multi frequency PLANCK data by Planck Collaboration et al. (2015) confirmed the power asymmetry and show that the foreground residuals are unlikely to affect these results. A multitude of other evidences favouring isotropy comes from isotropy in the angular distributions of radio sources (Wilson & Penzias 1967; Blake & Wall 2002), isotropy in the X-ray background (Wu et al. 1999; Scharf et al. 2000), isotropy of Gamma-ray bursts (Meegan et al. 1992; Briggs et al. 1996), isotropy in the distribution of galaxies (Marinoni et al. 2012; Alonso et al. 2015), isotropy in the distribution of supernovae (Gupta & Saini 2010; Lin et al. 2015) and isotropy in the distribution of neutral hydrogen (Hazra & Shafieloo 2015). Although large number of studies favour the statistical isotropy of the Universe on large scales there is no

★ E-mail: biswap@visva-bharati.ac.in

© 2015 The Authors

clear consensus on this issue yet. There are some studies with Type-Ia supernovae which find evidence for statistically significant anisotropy (Schwarz & Weinhorst 2007; Campanelli et al. 2011; Kalus et al. 2013; Javanmardi et al. 2015; Bengaly et al. 2015). Some other studies with radio sources (Jackson 2012) and galaxy luminosity function (Appleby & Shafieloo 2014) also point towards significant anisotropy. These anisotropies may originate from the systematics in the data. But there is also a possibility that they signal the failure of the assumption of cosmic isotropy itself. There would be a major paradigm shift in modern cosmology if the assumption of cosmic isotropy is ruled out with high statistical significance by multiple data sets. A large number of theoretical studies have been carried out on the possible origins of such anisotropy and their consequences (Chan et al. 2009; Shtanov 2010; Barrow & Hervik 2010; Soda 2012; Pitrou et al. 2008; Marozzi & Uzan 2012; Mukherjee et al. 2015).

Different statistics (Hajian & Souradeep 2003; Zunckel et al. 2011; Taylor & Gair 2013) has been developed to test isotropy for different types of data sets. Pandey (2013) introduce a method based on the Shannon entropy (Shannon 1948) for characterizing inhomogeneities in a 3D distribution of points and applied the method on some Monte Carlo simulations of inhomogeneous distributions and N-body simulations which show that the proposed method has great potential for testing the large scale homogeneity in galaxy redshift surveys. Recently Pandey & Sarkar (2015) applied this method to galaxy distributions from SDSS DR12 (Alam et al. 2015) and find that the inhomogeneities in the galaxy distributions persist at least upto a length scale of $120h^{-1}$ Mpc. A subsequent analysis of the SDSS LRG distribution (Eisenstein et al. 2001) by Pandey & Sarkar (2016) using an improved method reveal that the LRG distribution is homogeneous beyond length scales of $\sim 150h^{-1}$ Mpc. In the present work we propose a method for testing isotropy based on the Shannon entropy. The proposed method can be directly applied to 3D distributions of galaxies or the corresponding density fields derived from them. The method can be also easily extended to 2D maps such as CMB and may be also suitably adapted for testing isotropy of gravitational waves, cosmic rays, X-ray or Radio sky.

A brief outline of the paper follows. We describe our method in Section 2, describe the data and the tests in Section 3 and present the results in Section 4 and Conclusions in Section 5.

We have used a ΛCDM cosmological model with $\Omega_{m0} = 0.3$, $\Omega_{\Lambda 0} = 0.7$ and $h = 1$ throughout.

2 METHOD OF ANALYSIS

Pandey (2013) propose a method based on the Shannon entropy to study inhomogeneities in a 3D distribution of points. Shannon entropy (Shannon 1948) is originally proposed by Claude Shannon to quantify the information loss while transmitting a message in a communication channel. It gives a measure of the amount of information required to describe a random variable. The Shannon entropy for a discrete random variable x with n outcomes $\{x_i : i = 1, ...n\}$ is a measure of uncertainty denoted by $H(X)$ defined as,

$$H(X) = -\sum_{i=1}^{n} p(x_i) \log p(x_i) \tag{1}$$

where $p(x)$ is the probability distribution of the random variable x.

In the present work we propose information entropy as a measure of isotropy. We assume a set of points distributed in 3D and wish to test the assumption of statistical isotropy around any point. In order to test the isotropy around a point we first uniformly bin $\cos\theta$ and ϕ where θ and ϕ are the polar angle and azimuthal angle in spherical polar coordinates respectively. Uniform binning of $\cos\theta$ and ϕ ensure equal size for each solid angle bin since $d\Omega = \sin\theta d\theta d\phi$. The number of bins m_θ and m_ϕ for binning $\cos\theta$ and ϕ are to be decided conveniently. A given choice of m_θ and m_ϕ results in a total $m_{total} = m_\theta m_\phi$ solid angle bins. We impose an upper limit to the radius r upto which the isotropy is to be tested. There is a natural limit to r from the fact that the data points are available only upto a certain radius r_{max}.

We pick up a point about which isotropy has to be tested and treating that point as origin define the coordinates of all the other points in the distribution. We bin the co-ordinates for a given choice of m_θ, m_ϕ and r. This results in $m_{total} = m_\theta m_\phi$ volume elements each covering the same solid angle. For any given value of r each of the volume elements has the same radial extension ensuring same volume $dv = \frac{r^3}{3} d\Omega$ for each of them. We count the number of points n_i inside each of the m_{total} volume elements where i is the index of the volume element. In general each galaxy within radius r from the centre can reside in only one of the m_{total} volume elements. But which volume element a particular galaxy belongs to ? The answer to this question has m_{total} likely outcomes. We define a random variable $X_{\theta\phi}$ which has m_{total} possible outcomes each given by, $f_i = \frac{n_i}{\sum_{i=1}^{m_{total}} n_i}$ with the constraint $\sum_{i=1}^{m_{total}} f_i = 1$. The Shannon entropy associated with the random variable $X_{\theta\phi}$ can be written as,

$$\begin{aligned} H_{\theta\phi}(r) &= -\sum_{i=1}^{m_{total}} f_i \log f_i \\ &= \log N - \frac{\sum_{i=1}^{m_{total}} n_i \log n_i}{N} \end{aligned} \tag{2}$$

Where N is the total number of points within radius r. The base of the logarithm is arbitrary and we choose it to be 10. f_i will have the same value $\frac{1}{m_{total}}$ for all the volume elements when n_i is same for all of them. This maximizes the Shannon entropy to $(H_{\theta\phi})_{max} = \log m_{total}$ for a given choice of m_θ,m_ϕ and any r. We define the relative Shannon entropy as the ratio of the entropy of a random variable $X_{\theta\phi}$ to the maximum possible entropy $(H_{\theta\phi})_{max}$ associated with it. The relative Shannon entropy $\frac{H_{\theta\phi}(r)}{(H_{\theta\phi})_{max}}$ then quantifies the degree of uncertainty in the knowledge of the random variable $X_{\theta\phi}$. Equivalently $a_{\theta\phi}(r) = 1 - \frac{H_{\theta\phi}(r)}{(H_{\theta\phi})_{max}}$ quantify the residual information and can be treated as a measure of anisotropy. The fact that galaxies are not residing in any particular volume element and rather are distributed across all of them with different probabilities acts as a source of information. If all of them would have been residing in a particular volume

element then there would be no uncertainty and no information at all making $H_{\theta\phi} = 0$ or $a_{\theta\phi} = 1$. This fully determined situation corresponds to maximum anisotropy. On the other hand when all the m_{total} volume elements are populated with equal probabilities it would be most uncertain to decide which particular volume element a galaxy belongs to. This maximizes the information entropy to $H_{\theta\phi} = \log m_{total}$ turning $a_{\theta\phi} = 0$. This corresponds to a situation when the distribution is completely isotropic. The galaxy distribution is expected to be anisotropic on small scales but with increasing solid angle $d\Omega$ and radius r one would expect it to be isotropic on some scale provided the Cosmological principle holds on large scales. We change the value of r starting from a small radius r and gradually increase it in steps upto the maximum radius r_{max} to study how $a_{\theta\phi}(r)$ varies with r for a given choice of m_θ and m_ϕ. It may be noted here that the analysis can be also done for data covering parts of the sky.

We would like to mention here that the proposed measure of anisotropy would never be exactly zero and would be also sensitive to binning and sub-sampling. So we adopt a workable definition of isotropy where the distribution is considered to be isotropic when the measured anisotropy lies within the $1-\sigma$ errorbars of the anisotropy expected for a Poisson distribution. Consequently our preferred binning and sampling would be such that for which the anisotropy in the Poisson distribution decays to approximately zero within the scales probed.

Besides the radial anisotropy one can also measure the degree of polar anisotropy $a_\phi(\theta) = 1 - \frac{H_\phi}{(H_\phi)_{max}}$ and the azimuthal anisotropy $a_\theta(\phi) = 1 - \frac{H_\theta}{(H_\theta)_{max}}$ as function of θ and ϕ by carrying out the sum respectively over m_ϕ or m_θ instead of m_{total} in Equation 2. Note that in this case N would be the total number of points inside all the m_ϕ or m_θ volume elements at different θ or ϕ respectively. Note that $a_\phi(\theta)$ measures isotropy among all the ϕ bins at each θ and similarly $a_\theta(\phi)$ measures isotropy among all the θ bins at each ϕ. $a_\phi(\theta)$ and $a_\theta(\phi)$ are then determined at different θ and ϕ values respectively. One can also study $a_\phi(r)$ and $a_\theta(r)$ as a function of r at fixed θ and ϕ values respectively. However in the present work we only employ $a_{\theta\phi}(r)$, $a_\phi(\theta)$ and $a_\theta(\phi)$ to quantify and characterize the anisotropies present in a distribution.

It would be worth mentioning here that one can also estimate the variance in the number counts across the various volume elements in different (θ,ϕ) directions to measure the anisotropy present in a distribution. But we prefer entropy because unlike variance it is related to the higher order moments of a distribution. So in principle the entropy can be a better measure of non-uniformity than variance as it uses more information about the probability distribution. The Variance and the entropy would be equivalent as a measure of non-uniformity only when the probability distribution is fully characterized by the first two moments such as in a Gaussian distribution. However even all the higher order moments together can not uniquely describe a highly tailed distribution in the non-linear regime (Carron & Neyrinck 2012; Carron & Szapudi 2014). It has been suggested that the spectrum of the log-density field carries more information than the spectrum of the field and could be a better choice in such cases (Carron 2011).

When the probability distribution function is Gaussian then the associated Shannon entropy is $\log\sqrt{2\pi e}\sigma$ where σ is the standard deviation of the distribution. In ΛCDM model one can use the variance of the smoothed density field predicted from the power spectrum to estimate the Shannon entropy associated with that scale provided the density field is assumed to be Gaussian.

One can integrate $-\int p(x)\log p(x)dx$ for any probability distribution to estimate the associated differential entropy of the corresponding distribution. For example the differential entropy of the Poisson distribution is given by, $H(p_\lambda) = \lambda\log\frac{e}{\lambda} + e^{-\lambda}\sum_{k=0}^{\infty}\frac{\lambda^k\log k!}{k!}$, where λ is the average number of events per interval. In this case λ is the average number of points per volume element. Although the discrete entropy and differential entropy have similar mathematical forms there are some important differences between them. The differential entropy is not a number as in discrete entropy, but rather a function of one or more parameters that describes the associated probability distribution. The differential entropy does not provide the average amount of information contained in a random variable like its discrete counterpart. It is not an absolute measure of uncertainty rather it measures relative uncertainty or changes in uncertainty. One can show that the discrete entropy $H(x)_\Delta$ is related to the differential entropy $H(x)$ as, $H(x)_\Delta \approx H(x) - \log\Delta$ in the limit $\Delta \longrightarrow 0$ where Δ is the bin size used in discretization. The extra term $-\log\Delta$ approaches infinity as $\Delta \longrightarrow 0$. So one can only make relative comparisons of differential entropies and a simple comparison between the discrete entropy and the differential entropy is not quite meaningful (Michalowicz, Nichols & Bucholtz 2014).

The method presented here can be directly applied to different galaxy redshift surveys to test the isotropy of the galaxy distributions in the present Universe. The redshift surveys map the mass distribution on a light cone time slice where the distribution does not evolve much over the light crossing time of the survey. But for very large galaxy surveys possible evolutionary effects can introduce signatures of anisotropy in the data. Redshift dependent selection effects can also introduce artificial anisotropy in the data. Besides these the redshift space distortions is one of the most important source of anisotropy in galaxy surveys. On large scales structures are compressed along the line of sight due to coherent flows into overdense regions and out of underdense regions whereas on small scales structures are elongated along the line of sight by random motions in virialized clusters. The volume elements used for measurement of n_i in our method radially extends along the line of sight where the radial extension is much larger compared to their angular width. When measurements are done from the point from which observations are carried out one would expect uniformity in the measurement of n_i across all directions for large r provided the Universe is isotropic. But this would appear anisotropic if one shifts the origin from the point of observation given such sources of anisotropies are present. It is important to distinguish the presence of genuine anisotropies from the artificial ones such as introduced by radial inhomogeneities (due to selection effects, evolutionary effects) and redshift space distortions. We will show that our method can distinguish the signatures of different kind of anisotropies present in the distribution.

The method presented here has a significant advantage compared to the method proposed by Pandey (2013) for testing homogeneity using Shannon entropy. The volume elements used for measuring the number count n_i in this method do not overlap. Consequently all the complexities due to overlap can be bypassed allowing one to have a more direct and clear interpretation.

3 TESTING THE METHOD

In order to study the prospects and limitations of the proposed method we carry out some preliminary tests by applying it to some simple distributions. We consider the following distributions: (1) homogeneous and isotropic Poisson distributions, (2) anisotropic distributions generated by inserting pockets of different densities at different locations in homogeneous and isotropic Poisson distributions, (3) radially inhomogeneous Poisson distributions which are isotropic only about one point i.e. the centre and (4) simulated galaxy distributions from N-body simulations in real space and redshift space.

For the first three types we generate a set of Monte Carlo realizations. The distributions of type (1) are isotropic and type (2) are anisotropic by construction. The distributions of type (3) are radially inhomogeneous and the radial variations are identical in all directions making them isotropic about the centre of the sphere. But if we shift the origin from the centre of the sphere the distribution would appear anisotropic and the degree of anisotropy would depend on the magnitude and direction of the shift in a predictable manner. For the distributions of type (4) we use the data from a semi analytic galaxy catalogue from the Millennium simulation. An isotropic distribution in real space would appear anisotropic in redshift space due to redshift space distortions induced by the peculiar velocities. We map the particles in N-body simulations from real space to redshift space using their peculiar velocities and measure the resulting anisotropies induced by redshift space distortions. In all cases we have considered a spherical region of radius $200h^{-1}\,\mathrm{Mpc}$.

We analyze the datasets separately using the method described in section 2. We divide the $\theta-\phi$ space into $m_\theta m_\phi$ solid angle bins where m_θ and m_ϕ are variables and chosen conveniently. The following calculations are carried out for each of the datasets described in the subsections below.

(i) We choose the minimum and maximum values of radius r to be $r_{min} = 5h^{-1}\,\mathrm{Mpc}$ and $r_{max} = 200h^{-1}\,\mathrm{Mpc}$. We gradually increase the radius r in steps of $5h^{-1}\,\mathrm{Mpc}$ from r_{min} to r_{max} and compute the Shannon entropy $\frac{H_{\theta\phi}}{(H_{\theta\phi})_{max}}$ for each radius using all the available $m_\theta m_\phi$ bins.

(ii) We fix the radius at $r_{max} = 200h^{-1}\,\mathrm{Mpc}$ and compute $\frac{H_\theta}{(H_\theta)_{max}}$ for each θ using all the m_ϕ azimuthal bins available.

(iii) We fix the radius at $200h^{-1}\,\mathrm{Mpc}$ and compute $\frac{H_\phi}{(H_\phi)_{max}}$ for each ϕ using all the m_θ polar bins available.

(iv) We shift the origin by $100h^{-1}\,\mathrm{Mpc}$ along the x-axes without any rotation and repeat (i),(ii) and (iii) using $r_{max} = 100h^{-1}\,\mathrm{Mpc}$.

(v) We shift the origin by $100h^{-1}\,\mathrm{Mpc}$ along the y-axes without any rotation and repeat (i),(ii) and (iii) using $r_{max} = 100h^{-1}\,\mathrm{Mpc}$.

(vi) We shift the origin by $100h^{-1}\,\mathrm{Mpc}$ along the z-axes without any rotation and repeat (i),(ii) and (iii) using $r_{max} = 100h^{-1}\,\mathrm{Mpc}$.

In general one can apply the shift along any arbitrary directions and it would not make any difference given the distribution is isotropic. Further if one can verify the isotropy around other points it would also help us in testing homogeneity of the distribution.

3.1 MONTE CARLO SIMULATIONS

The Monte Carlo simulations for the data sets of type (1) and (3) are generated by considering two simple radial density distributions $\rho(r,\theta,\phi) = K\lambda(r)$ where $\lambda(r) = 1$ for type (1) and $\lambda(r) = \frac{1}{r^2}$ for type (3) distributions. Here K is a normalization constant. The type (1) distributions are homogeneous and isotropic Poisson point process which has a constant density everywhere. The type (3) distributions are radially inhomogeneous Poisson distributions which are isotropic only about the centre.

Enforcing the desired number of particles N within radius R one can turn the radial density function into a probability function within $r = 0$ to $r = R$ which is normalized to one when integrated over that interval. So the probability of finding a particle at a given radius r is $P(r) = \frac{r^2\lambda(r)}{\int_0^R r^2\lambda(r)dr}$ which is proportional to the density at that radius implying more particles in high density regions.

We generate the Monte Carlo realizations of these distributions using a Monte Carlo dartboard technique. The maxima of the function $r^2\lambda(r)$ in $P(r)$ is at $r = R$ for type (1) distribution whereas in type (3) distribution it is same and constant everywhere. We label the maximum value of $P(r)$ as P_{max}. We randomly choose a radius r in the range $0 \le r \le R$ and a probability value is randomly chosen in the range $0 \le P(x) \le P_{max}$. The actual probability of finding a particle at the selected radius is then calculated using expression for $P(r)$ and compared to the randomly selected probability value. If the random probability is less than the calculated value, the radius is accepted and assigned isotropically selected angular co-ordinates θ and ϕ, otherwise the radius is discarded. In this way, radii at which particle is more likely to be found will be selected more often because the random probability will be more frequently less than the calculated actual probability. We choose $R = 200h^{-1}\,\mathrm{Mpc}$ and $N = 10^5$.

To generate the distributions of type (2) we first generate a homogeneous and isotropic Poisson distribution within a spherical region of radius $200h^{-1}\,\mathrm{Mpc}$ with $N = 10^5$. We randomly identify a region in (r,θ,ϕ) space assuming the centre of the sphere as origin. We discard all the data points from the selected region and subsequently populate it with a homogeneous and isotropic Poisson distribution having a different intensity parameter than the original one. As a result this region will have a different mean density which introduces a preferred direction and hence anisotropy in the distribution.

We generate 10 realizations for each of the above density distributions and analyze them separately using the method described earlier.

3.2 MILLENNIUM SIMULATION

Semi analytic models (White & Frenk 1991; Kauffmann, White & Guiderdoni 1993; Kauffmann & White 1993; Kauffmann 1996; Cole et al. 1994, 2000; Somerville & Primack 1999; Baugh et al. 1998; Benson et al. 2002; Springel et al. 2005; Guo et al. 2011) provide a very powerful tool to study galaxy formation and evolution. Galaxy formation and evolution involve many physical processes such as gas cooling, star formation, supernovae feedback, metal enrichment, merging and morphological evolution. The semi analytic models parametrise the physics involved in terms of simple models following the dark matter merger trees over time. The models provide the statistical predictions of galaxy properties at some epoch and the precision of these predictions are directly related to the accuracy of the input physics. In the present work we use a semi-analytic galaxy catalogue generated by Guo et al. (2011) from the Millennium Run simulation(Springel et al. 2005) who updated the previously available galaxy formation models (Springel et al. 2005; Croton et al. 2006; De Lucia & Blaizot 2007) with improved versions. The spectra and magnitude of the model galaxies were computed using population synthesis models of Bruzual & Charlot (2003). We place the origin at the centre of the simulation box which has a length of $500h^{-1}$ Mpc on each side and then identify all the galaxies within a radius of $200h^{-1}$ Mpc having r-band Petrosian absolute magnitude in the range $-22 \leq M_r \leq -20$. We randomly select 10^5 galaxies from them to construct the simulated galaxy sample in real space for our analysis. We then map these galaxies to redshift space using their peculiar velocities to obtain their distribution in redshift space.

4 RESULTS

We show the results for the homogeneous and isotropic Poisson distributions in Figure 1. In top left, middle left and bottom left panels we show the degree of anisotropies as a function of r, θ and ϕ respectively. The top left panel shows the variations of $a_{\theta\phi}(r)$ (hereafter radial anisotropy) as a function of r for different choices of m_θ and m_ϕ. At the smallest radius one finds a large anisotropy arising purely from Poisson noise which gradually diminishes with increasing radii. This result holds for all choices of m_θ and m_ϕ but for larger values of m_θ and m_ϕ the anisotropies resulting from Poisson noise are larger and persist upto larger length scales. This arises simply because with increasing m_θ and m_ϕ the solid angle bins cover smaller volumes and hence contain fewer points within for any given r. The middle left panel shows the variations of $a_\phi(\theta)$ (hereafter polar anisotropy) as a function of θ for different choices of m_θ and m_ϕ labeled in the panel. We note that for $m_\theta = 10$ and $m_\phi = 20$ we uniformly get $a_\phi(\theta) \approx 0$ for all values of θ indicating isotropy of the distribution. But as we increase the total number of bins by 10^2 times $(m_\theta = 100, m_\phi = 200)$ and 10^4 times $(m_\theta = 1000, m_\phi = 2000)$ the anisotropies resulting from the Poisson noise become evident. The degree of anisotropy increases with increasing number of bins for all θ but does not change with θ indicating a systematic behaviour as expected from Poisson noise. We notice exactly same behaviour for $a_\theta(\phi)$ (hereafter azimuthal anisotropy) as a function of ϕ in the bottom left panel confirming isotropy of the distribution. The entropy of a 3D Poisson point process would depend on λ which is the average number of points expected in a volume element in each binning schemes. We see a variation in the radial anisotropy $a_{\phi\theta}(r)$ with increasing r as λ changes with increasing radii whereas $a_\phi(\theta)$ and $a_\theta(\phi)$ do not change with θ and ϕ since λ remains constant in any specific binning schemes. The standard deviations in the values of $a_{\phi\theta}(r)$, $a_\phi(\theta)$ and $a_\theta(\phi)$ increase with increasing number of bins following the characteristics of Poisson noise.

In the top, middle and bottom right panels we show how the anisotropies vary with r, θ and ϕ respectively for different choices of m_θ and m_ϕ when the origin is shifted by $100h^{-1}$ Mpc along the x or y or z axes without any rotation. It may be noted here that we can only probe upto a length scale of $100h^{-1}$ Mpc under these circumstances. We set $r_{max} = 100h^{-1}$ Mpc in each of these cases. In the top right panel we see that the $a_{\theta\phi}(r)$ remain unaltered when the origin is shifted by $100h^{-1}$ Mpc along the x, y and z axes or not shifted at all indicating the isotropy of the distribution. This result holds for each set of m_θ and m_ϕ. In the right middle panel we show $a_\phi(\theta)$ as a function of θ when the origin is not shifted and when the origin is shifted along three different directions. Interestingly the results overlap with each other again pointing towards isotropy of the distribution. One may note here that the degree of anisotropy and the size of the errorbars increase at a fixed choice of m_θ and m_ϕ due to the decrease in r_{max} resulting in a smaller number of points within the volumes analyzed. In the bottom right panel $a_\theta(\phi)$ as a function of ϕ shows identical behaviour showing isotropy of the distribution in ϕ and rise in anisotropy with increase in the number of bins. Here the error bars are derived from 10 different Monte Carlo realizations in each case. We are interested in finding out the genuine signals of anisotropy. So keeping in mind the role of Poisson noise in increasing the anisotropy and the size of error-bars we decide to use $m_\theta = 10$ and $m_\phi = 20$ for the rest of our analysis. One can of course safely increase m_θ and m_ϕ by increasing the density of the distribution at the same time.

We introduce an empty pocket in the homogeneous and isotropic Poisson distribution by removing all the points from the region $80h^{-1}$ Mpc $\leq r \leq 180h^{-1}$ Mpc, $90^\circ \leq \theta \leq 140^\circ$ and $90^\circ \leq \phi \leq 190^\circ$. This introduces a directional asymmetry in the resulting distribution. Subsequently we fill up the empty pocket by generating another homogeneous and isotropic Poisson distribution within it which has a different density than the original one. We considered two distinct case, one in which we doubled the density and another in which we halved the density with respect to the original distribution. We analyze 10 such Monte Carlo realizations in each case. The results are shown in Figure 2. We show the radial anisotropy as a function of r for $m_\theta = 10$ and $m_\phi = 20$ in the top left panel of Figure 2. As seen earlier in Figure 1 once again we see a higher degree of anisotropy on small scales due to the Poisson noise. The anisotropy decreases with increasing length scales when there is no pocket in the distribution. But in the presence of the pocket described above the anisotropies reappear again at $80h^{-1}$ Mpc and persists thereafter. It may be noted here that the pocket introduced radially extends from $80h^{-1}$ Mpc to $180h^{-1}$ Mpc from the centre.

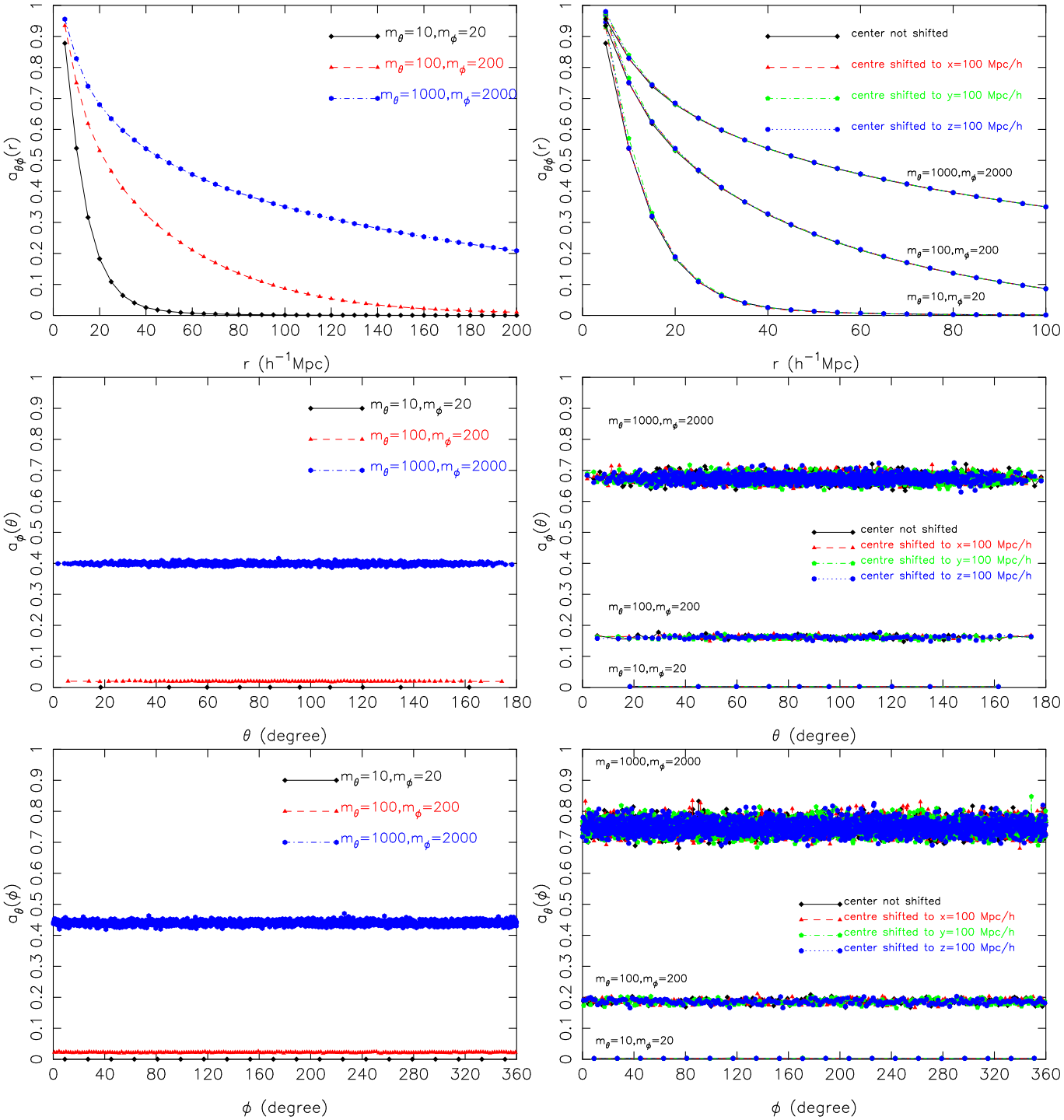

Figure 1. The top left, middle left and bottom left panels show the measured anisotropies in a homogeneous and isotropic Poisson distribution as functions of r, θ and ϕ respectively for different choices of m_θ and m_ϕ as labeled in each panel. The top right, middle right and bottom right panels show the same quantities when the origin is shifted along x or y or z directions from the centre by $100h^{-1}$ Mpc. We use $r_{max} = 200h^{-1}$ Mpc and $r_{max} = 100h^{-1}$ Mpc for all the panels on left and right respectively. The level of anisotropy seen in each panel correponds to the errors arising due to the discrete nature of the sampling. One needs to take into account these errors while testing for isotropy of any distribution with the same sampling rate and number of bins. The rest of our analysis are done at the same sampling rate and we use $m_\theta = 10$ and $m_\phi = 20$. We refer to these errors in the next figures.

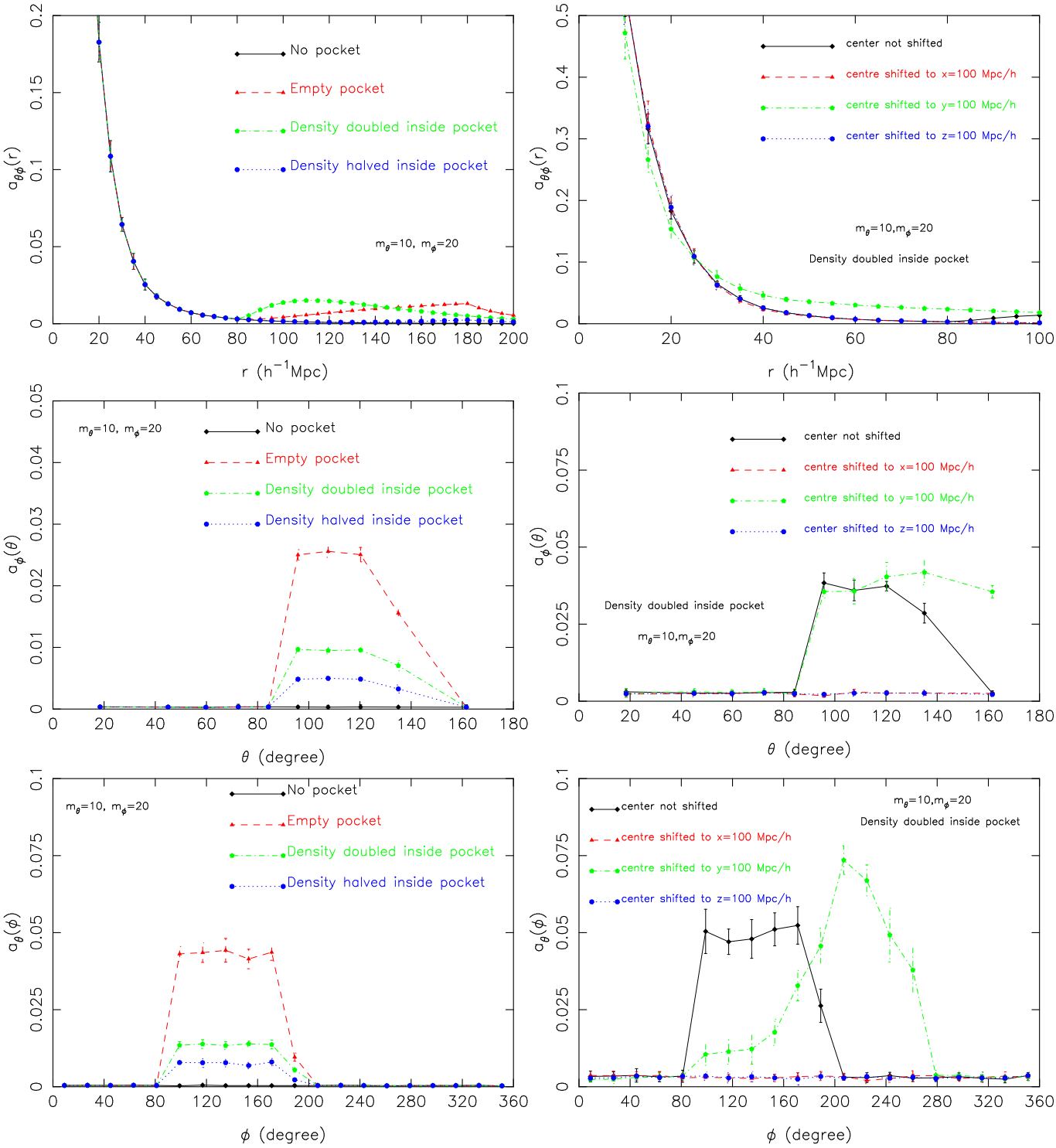

Figure 2. Same as Figure 1. but for anisotropic Poisson distribution obtained by introducing pocket of different density in a homogeneous and isotropic Poisson distribution. Only the results for $m_\theta = 10$ and $m_\phi = 20$ are shown in each panel. The error-bars shown here in all the panels are the $1-\sigma$ variations from the 10 Monte Carlo realizations used in each case. The results for 'No pocket' corresponds to the anisotropy level resulting from discreteness in a homogeneous and isotropic Poisson distribution. In all these cases the geometry of the pocket introduced are following: $80h^{-1}\,\mathrm{Mpc} \le r \le 180h^{-1}\,\mathrm{Mpc}$, $90^\circ \le \theta \le 140^\circ$, $90^\circ \le \phi \le 190^\circ$.

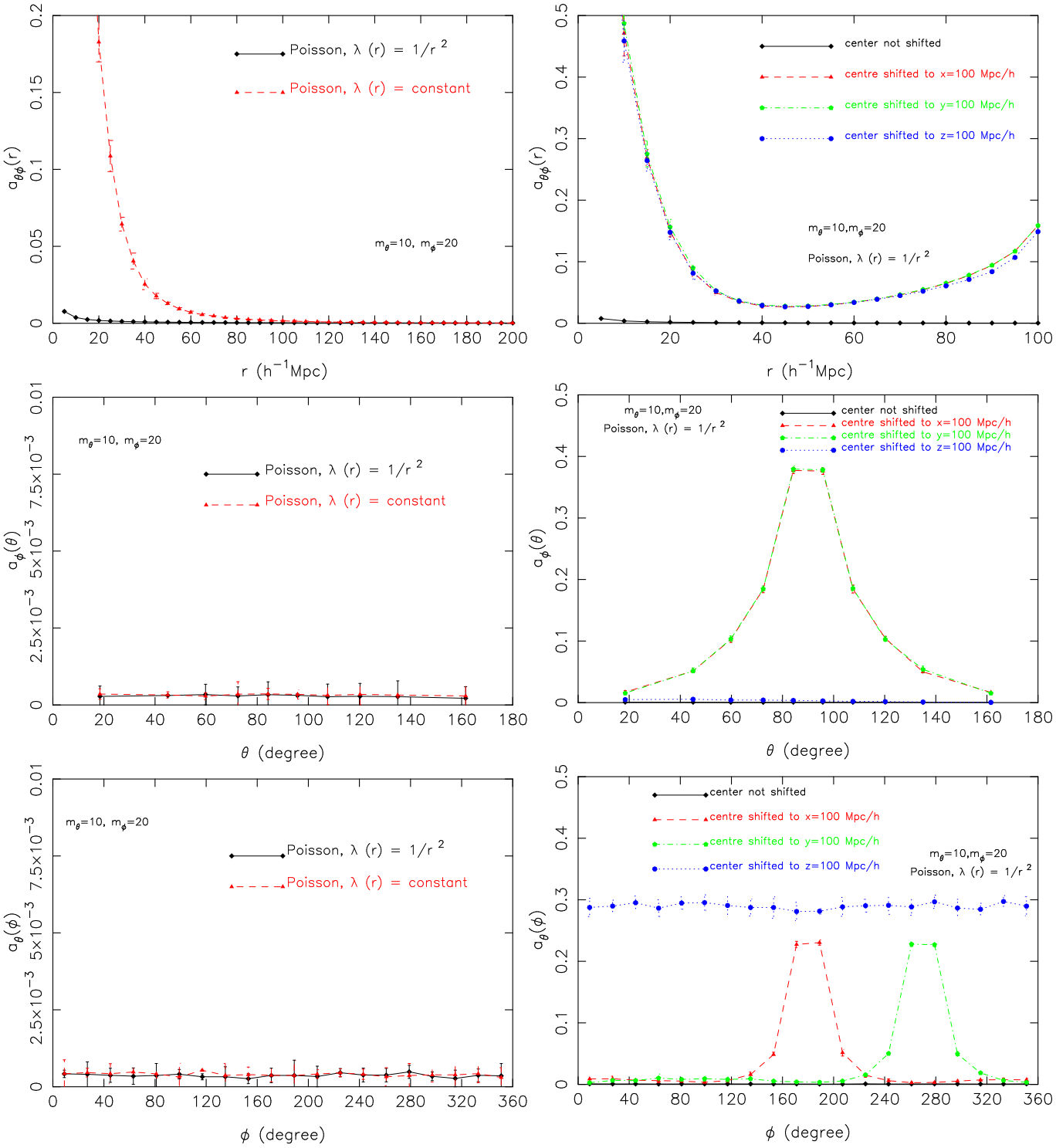

Figure 3. Same as Figure 1. but for radially inhomogeneous Poisson distribution where density varies as $\frac{1}{r^2}$ from the centre. Only the results for $m_\theta = 10$ and $m_\phi = 20$ are shown in each panel. The error-bars shown here in all the panels are the $1-\sigma$ variations from the 10 Monte Carlo realizations used in each case. The results for 'Poisson, $\lambda(r)$ =constant' corresponds to the anisotropy level resulting from discreteness in a homogeneous and isotropic Poisson distribution.

We note that the signals of anisotropy in this range of radii are less pronounced when the density of points are halved than when doubled or when the pocket is left empty. The left middle and left bottom panel show the polar anisotropy as a function of θ and azimuthal anisotropy as a function of ϕ respectively. In the left middle panel we see a clear and distinct bump in the polar anisotropy in the θ range 90° to 160° when the pocket is introduced in the distribution. Noticeably the bump is absent when no such pockets are introduced. For all other θ values we uniformly get $a_\phi(\theta) \approx 0$. The height of

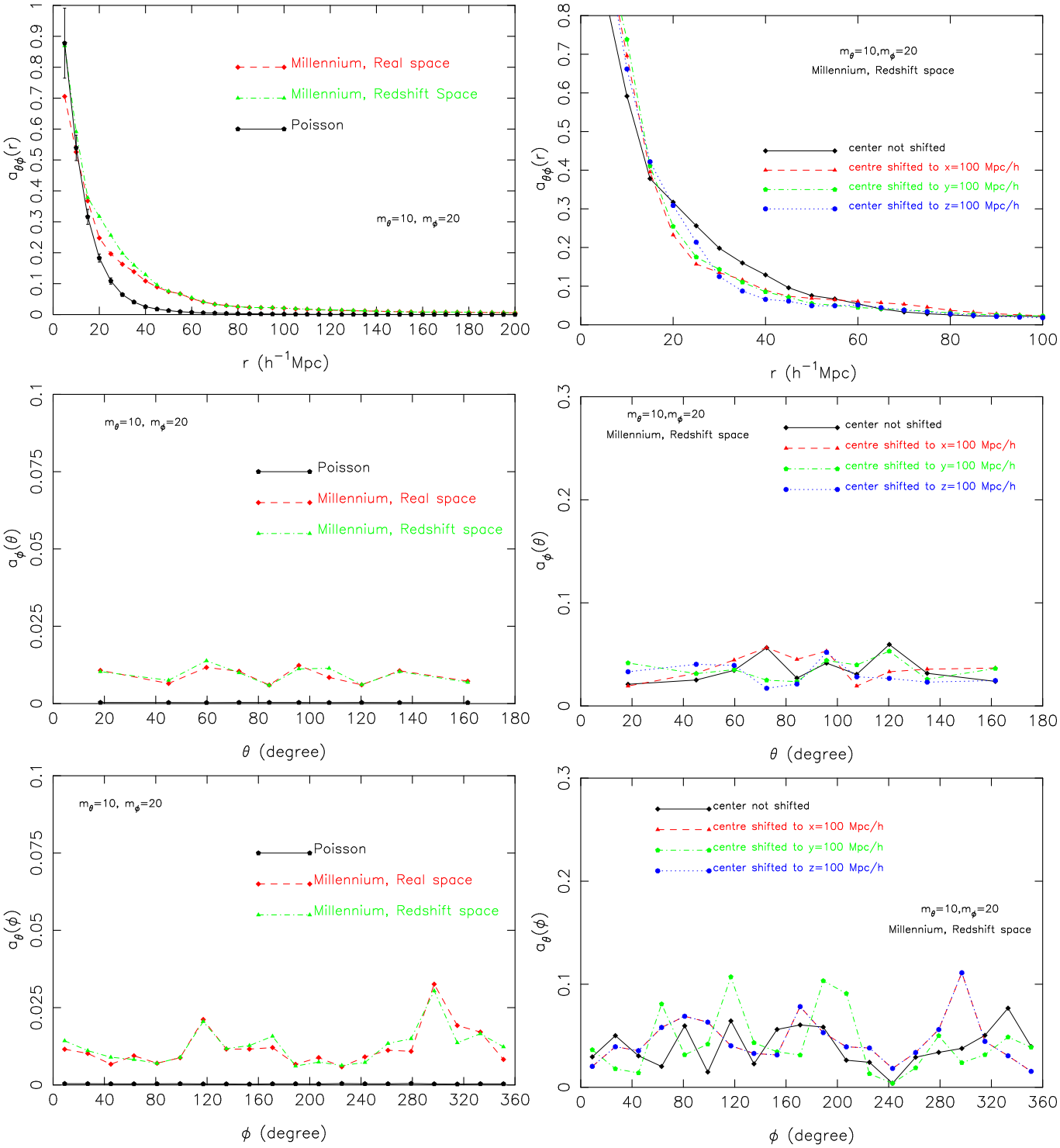

Figure 4. Same as Figure 1. but for simulated galaxy distributions from a semi analytic galaxy catalogue from the Millennium Run simulation. The panels on left side compares the results for the real space and redshift space whereas the panels on right only show the results for the redshift space. The error-bars shown for the homogeneous and isotropic Poisson distributions are the $1-\sigma$ variations from the 10 Monte Carlo realizations. No error-bars are shown for the galaxies from the Millennium simulation as we have only one galaxy sample from it.

the bump quantifies the degree of anisotropy and depends on the number density inside the pocket. The bump clearly indicates violation of isotropy in the range of θ values over which it appears. Interestingly the pocket generated spans exactly the same range of θ over which the bump appears. Consequently one can infer the size of the pocket from the features of the bump. The fact that the the bumps extend upto $160h^{-1}$ Mpc rather $140h^{-1}$ Mpc is due to the fact the next θ bin after 135° falls only at $\sim 160^\circ$. The angular span of the pocket in θ can be more accurately determined using a larger number of θ bins. The signal of anisotropy is strongest when the pocket is left empty and decreases when the pocket is filled with a homogeneous and isotropic Poisson distribution with a different density than the original one. We then compare the degree of anisotropy when the pocket is filled with twice and half the density of the original distribution. It is interesting to note that the signals of anisotropy gets stronger with increasing density as it increases the disparity of the density inside the pocket from the original one. The anisotropy signals completely disappear when the pocket is filled with points having same density as the original one. In the left bottom panel we show the anisotropy as a function of azimuthal angle ϕ and similarly find $a_\theta(\phi) \approx 0$ for all ϕ values other than the range $90^\circ \leq \phi \leq 190^\circ$ where $a_\theta(\phi) > 0$ produce a bump in the azimuthal anisotropy. This bump-like feature in the azimuthal anisotropy indicates violation of isotropy in the direction $90^\circ \leq \phi \leq 190^\circ$ in presence of the pocket. Interestingly the pocket introduced has the same angular span in ϕ. Clearly the bump does not appear in the absence of any such pocket. The presence of the pocket violates the isotropy of the distribution and is marked by the appearance of the bumps in the radial, polar and azimuthal anisotropies. Combining these information one can exactly infer the geometry of the pocket violating isotropy and also infer the degree of anisotropy due to it from the height of the bumps. Here we would like to mention that for an arbitrary shape of the pocket it is not trivial to figure out its exact geometry using the current method.

Next we consider only the set of distributions where the pocket is filled with a homogeneous and isotropic Poisson distribution having density twice than that of the original one. We again separately measure anisotropies as a function of r, θ and ϕ from multiple points of observation inside the distribution. We shift the origin along x, y and z directions by $100h^{-1}$ Mpc without any rotation of the axes to have three different point of observations. We compare our findings in the top right, middle right and bottom right panels of Figure 2. In the top right panel of Figure 2 we show the anisotropy as a function of r for the cases where the centre is shifted along x, y or z directions or not shifted at all. We find that the variations in anisotropy are identical in all cases except when the origin is shifted along y direction. This is due to the fact that the geometry of the pocket ($80h^{-1}$ Mpc $\leq r \leq 180h^{-1}$ Mpc, $90^\circ \leq \theta \leq 140^\circ$, $90^\circ \leq \phi \leq 190^\circ$) does not affect the measurements in any of these cases other than when the shift is applied along y direction. This shows the existence of a preferred direction which clearly violates isotropy. This becomes even clearer in the right middle and right bottom panels of Figure 2. In the right middle panel we see that a bump appears between 90° to 160° when the centre is not shifted. The pocket radially spans from $80-180h^{-1}$ Mpc and hence overlaps with the current measurement producing an anisotropy signal in the appropriate range of θ. On the other hand the pocket is completely excluded from the measurements when the centre is shifted along x or z directions showing a near uniform very small signal of anisotropy for all θ values. This small signal of anisotropy arises due to the Poisson noise resulting simply from the reduction in the radial extensions of the volume elements used in the measurements. But when we shift the origin along y direction by $100h^{-1}$ Mpc the measurements include major part of the pocket showing anisotropy in the relevant range of θ. As there are no rotations of the axes, the bump appears exactly at $\theta = 90^\circ$ irrespective of whether the centre is shifted along y direction or not shifted at all. But the shifted position of the origin redefines the geometry of the pocket which changes the upper limit of θ for the pocket when the centre is shifted along y direction. We see very similar results in the right bottom panel of Figure 2 where anisotropies are shown as a function of ϕ. We again find presence of bumps over the appropriate range of ϕ values when the centre is shifted along y directions or not shifted at all whereas the distribution appears to be isotropic when the origin is shifted along x or z directions. These differences clearly indicate the presence of anisotropies in the distribution. The error-bars shown here in all the panels are the $1-\sigma$ variations from the 10 Monte Carlo realizations used in each case.

For the inhomogeneous Poisson distributions the density only varies radially as $\frac{1}{r^2}$ from the centre. This preserves the isotropy of the distribution about the centre but isotropy is violated for all other points. We want to test if our method can capture these expected behaviours for such distributions. The results are shown in different panels of Figure 3. In top left panel we show the anisotropy as a function of radial distance r when the origin is located at the centre of the spherical volume. When we compare the anisotropy in the homogeneous and radially inhomogeneous Poisson distributions we find that the former shows a higher degree of anisotropy than the later. The inhomogeneous Poisson distribution considered here has a radial variation in density as $\frac{1}{r^2}$ from the centre. As a result the number density of points are significantly higher at smaller radii in the inhomogeneous Poisson distribution as compared to the homogeneous one. This leads to significant reduction in the Poisson noise at smaller radii where it is considered to be more dominant. At larger radii the situation would be just opposite but as the number counts are cumulative in our method the distribution would remain isotropic as expected despite the radial decrease in density. In the middle left and bottom left panels of Figure 3 we show the anisotropies as function of θ and ϕ respectively. In both cases we have used $r_{max} = 200h^{-1}$ Mpc. We find that as expected the distributions are found to be highly isotropic from the centre.

The top right panel of Figure 3 shows the anisotropies as a function of r when the origins are shifted from the centre by $100h^{-1}$ Mpc along x or y or z direction. We see a large anisotropy at smaller radii which decreases with increasing radii due to the relative increase in the number counts and again increases afterwards due to large disparity in the density at the central and peripheral regions. The variations in anisotropies are identical when the origin is shifted from the centre along x, y or z directions due to the identical variations in density along all radial directions but they are noticeably different from the results obtained without shifting

the origin from the centre. This demonstrates the anisotropic nature of the distribution.

The middle right panel of Figure 3 show the anisotropies as a function of θ when the origin is shifted in various directions. It is interesting to note that when we shift the origin along z direction the distribution appears to be isotropic in θ as it would appear without any shift at all. The relative Shannon entropy is measured across all the ϕ bins at each θ values. The polar angle θ is defined with respect to the z axis and all the ϕ bins at a specific θ value are located at the same distance from the centre. Since the density only changes in the radial directions the distribution would appear isotropic in all ϕ directions for each θ when the origin is shifted in the z direction. The situations are not analogous when the origin is shifted in the x or y direction. In both the cases different ϕ bins at any given θ value are located at different distances from the centre leading to variations in their densities. This is true for all θ values albeit with a different degree of variation. The degree of variation across all the ϕ bins is expected to peak at $\theta = 90^\circ$ as it would encompass largest variation in the radial distances among the ϕ bins. Interestingly our method capture these predictable behaviours of anisotropies as a function of θ quite well.

Finally in the bottom right panel of Figure 3 we show the anisotropies as a function of ϕ. Here we estimate the relative Shannon entropy utilizing the information across all the θ bins at each ϕ values. When the origin is shifted in z direction the azimuthal angle ϕ is redefined in the shifted x-y plane which lies at a fixed distance $100h^{-1}$ Mpc from the centre. Consequently different θ bins at any given ϕ value are at different distances from the centre leading to variations in their densities but the degree of variations across the different θ bins for each ϕ value would be exactly same as the θ bins cover same variations in their radial distances. In the bottom right panel we see a constant degree of anisotropy across all the ϕ values when the origin is shifted along z direction. On the other hand when the origin is shifted along x or y direction the available θ bins at each ϕ value are located at different distances from the centre. As a result the different θ bins at each ϕ values would exhibit different number density depending on their distances from the centre. But the degree of variations would not be same for all the ϕ bins as it depends both on the distance range covered by the corresponding θ bins as well as if those θ bins lie towards or away from the centre. Clearly these variations are expected to peak at $\phi = 180^\circ$ and $\phi = 270^\circ$ for shift along x and y directions respectively. We exactly recover these predictable behaviours in the bottom right panel. Differences in the anisotropies with shifts and without shift clearly indicate that the distribution is anisotropic in nature. These results together indicate that our method is not only able to sense the anisotropies but also can capture the nature of anisotropies present in a distribution.

In Figure 4 we investigate the anisotropies resulting from the redshift space distortions using a semi analytic galaxy catalogue from the Millennium Run simulation. In the top left panel of this figure we compare the anisotropies as a function of radius r for the simulated galaxy distributions in real and redshift space. Both distributions show anisotropies on small scales which partly arise due to inevitable Poisson noise. The degree of anisotropy gradually decreases with increasing radii. Noticeably at smaller radii the degree of anisotropy in both the distributions are higher as compared to a homogeneous and isotropic Poisson distribution indicating the presence of additional sources of anisotropy other than the Poisson noise. We see that on smaller radii the redshift space distribution of the simulated galaxies are more anisotropic than its real space counterpart. This is most likely caused due to the elongation of virialized clusters, compression of large scale overdensities and elongation of large scale underdensities along the line of sight in redshift space. The results clearly indicate that distribution of galaxies inside the cosmic web is not isotropic even in real space and redshift space distortions only enhance these anisotropies further. The differences between the real space and redshift space anisotropies cease to exist beyond $40h^{-1}$ Mpc and both the anisotropies become almost indistinguishable from that observed in homogeneous and isotropic Poisson distributions at $\sim 140h^{-1}$ Mpc. It may be worth mentioning here that in an earlier work (Pandey & Sarkar 2015) we find that observed galaxy distribution in the SDSS DR12 appears to be homogeneous on scales above $140h^{-1}$ Mpc. In the middle left and bottom left panels of Figure 4 we show the anisotropies as a function of θ and ϕ respectively. In both these panels we find that the real and redshift space distributions are equally isotropic in θ and ϕ. A small signal of anisotropy exist for both real and redshift space distributions of the simulated galaxies which separates them from identical homogeneous and isotropic Poisson distributions. The real and redshift space distributions demonstrate equal degree of isotropy both in θ and ϕ due to the fact that the compression and elongation of overdense and underdense regions are symmetric along the line of sight. We use $r_{max} = 200h^{-1}$ Mpc for all the results shown in all the panels on left of Figure 4.

Now we shift the origin from the centre along the x or y or z axis by $100h^{-1}$ Mpc in the redshift space distribution of the simulated galaxies. The resulting anisotropies as a function of r, θ and ϕ are shown in the top right, middle right and bottom right panels of Figure 4 respectively. We see in the top right panel of Figure 4 that the observed anisotropies change at smaller radii when the origin is shifted along x, y or z directions than when it is not shifted. This tells us that the distribution is anisotropic under such shifts. In the middle right and bottom right panels we show the anisotropies in analogous situations but as functions of θ and ϕ respectively. The results in these panels show that the resulting anisotropies under such shifts and without shift appears to be similar when measured as functions of θ and ϕ whereas the level of anisotropies are expected to be different in this case when the origin is shifted from the centre. The top right panel of Figure 4 agrees quite well with this expected behaviour but the middle right and bottom right panels do not exhibit these differences. The redshift space distortions are caused by the radial component of peculiar velocities which distorts the structures along the line of sight. The method presented here may not be able to capture the anisotropies imprinted in the details of distortions when looked in the polar and azimuthal directions as we are currently using only the number counts within the solid angle bins which radially extends upto r_{max}. Using the correlation functions instead of number counts may prove to be a better bet here.

5 CONCLUSIONS

We present an information theory based method for testing isotropy in a three dimensional distribution and test the method on some Monte Carlo simulations of isotropic and anisotropic distributions. We find that our method can effectively identify and characterize various types of anisotropies and distinguish between them. We insert pockets of different densities inside homogeneous and isotropic distributions and find that the proposed method can effectively quantify the degree of the resulting anisotropy and also determine the geometry of the pockets introduced. We also consider spherically symmetric radially inhomogeneous distributions and find that such anisotropy can be easily characterized by our method. We then study the anisotropies induced by the redshift space distortions by using a semi analytic galaxy catalogue from the Millennium simulation and find that the method can separate such anisotropies from a general one. But in general the distributions could be much more complex specially when the observed anisotropy results from different possible combinations of various types of anisotropies. Disentangling such anisotropies is no doubt would be quite challenging. However our method could serve the purpose of detecting anisotropies quite well. In future we plan to analyze data from the Two Micron All Sky Survey (2MASS) and the Sloan Digital Sky Survey (SDSS) to test the assumption of isotropy in the present Universe.

One may also extend the present method in Fourier space. In this case one requires to estimate the PDF of the Fourier mode amplitudes in different volume elements and then apply the anisotropy measures presented here. Alternatively one can compute the Kullback-Leibler divergence of the PDF of the Fourier mode amplitudes across the various volume elements to identify and assess any power asymmetry. One may also quantify the phase entropy by defining an information entropy on the set of Fourier phases in different hemispheres and then compare the information content across different hemispheres. The degree of non-uniformity in the level of phase information could be used as a measure of anisotropy in this case.

An important caveat in the present method arises from the tiling strategy adopted here. The $\theta - \phi$ scheme that we have implemented here ensure identical sizes for all the volume elements but they do not have identical shapes which make the prediction of anisotropy difficult in general. A HEALPix tessellation (Gorski et al. 1999; Górski et al. 2005) would be more appropriate and useful while analyzing observations. We plan to incorporate the HEALPix scheme into our method in its future applications to galaxy surveys.

The proposed method can be also applied in many problems in Cosmology which requires tests of isotropy. For example it can be used to investigate the issues like the anisotropic distribution of galactic satellites (Zentner et al. 2005) and anisotropic distribution of subhalos inside dark matter halos and the cosmic web (Kang & Wang 2015). The method can be also used further to test for any hemispherical asymmetry in the angular distribution of galaxy clusters (Bengaly et al. 2015) and gamma-ray bursts (Briggs et al. 1996). Finally we note that the method presented here has the desired ability to identify and characterize any signals of anisotropy present in a distribution and it can be also suitably adapted for different types of datasets from other cosmological observations to efficiently explore the issue of Cosmic isotropy.

6 ACKNOWLEDGEMENT

I sincerely thank an anonymous referee for a thorough review with constructive suggestions which significantly helped to improve the draft. The author would like to acknowledge CTS, IIT Kharagpur for the use of its facilities for the present work. The author would also like to acknowledge IUCAA, Pune for providing support through the Associateship Programme.

The Millennium Simulation data bases (Lemson & Virgo Consortium 2006) used in this paper and the web application providing online access to them were constructed as part of the activities of the German Astrophysical Virtual Observatory.

REFERENCES

Ahn, C. P., Alexandroff, R., Allende Prieto, C., et al. 2014, ApJS, 211, 17
Alam, S., Albareti, F. D., Allende Prieto, C., et al. 2015, arXiv:1501.00963, Accepted to ApJS
Alonso, D., Salvador, A. I., Sánchez, F. J., et al. 2015, MNRAS, 449, 670
Appleby, S., & Shafieloo, A. 2014, JCAP, 10, 070
Baugh, C.M., Cole, S., Frenk, C.S. & Lacey, C.G. 1998, ApJ, 498, 504
Barrow, J. D., & Hervik, S. 2010, Physical Review D, 81, 023513
Bengaly, C. A. P., Jr., Bernui, A., & Alcaniz, J. S. 2015, ApJ, 808, 39
Bengaly, C. A. P., Jr., Bernui, A., Alcaniz, J. S., & Ferreira, I. S. 2015, arXiv:1511.09414
Benson, A.J., Lacey, C.G., Baugh, C.M., Cole, S. & Frenk, C.S. 2002, MNRAS, 333, 156
Bennett, C. L., Hill, R. S., Hinshaw, G., et al. 2011, ApJS, 192, 17
Blake, C., & Wall, J. 2002, Nature, 416, 150
Briggs, M. S., Paciesas, W. S., Pendleton, G. N., et al. 1996, ApJ, 459, 40
Bruzual, G., & Charlot, S. 2003, MNRAS, 344, 1000
Buchert, T., & Ehlers, J. 1997, A&A, 320, 1
Buchert, T. 2001, General Relativity and Gravitation, 33, 1381
Campanelli, L., Cea, P., Fogli, G. L., & Marrone, A. 2011, Physical Review D, 83, 103503
Carron, J., & Neyrinck, M. C. 2012, ApJ, 750, 28
Carron, J. 2011, ApJ, 738, 86
Carron, J., & Szapudi, I. 2014, MNRAS, 439, L11
Chan, R., da Silva, M. F. A., & Villas da Rocha, J. F. 2009, Modern Physics Letters A, 24, 1137
Cole, S., Aragon-Salamanaca, A., Frenk, C.S., Navarro, J.F., Zepf, S.E. 1994, MNRAS, 271, 781
Cole, S., Lacey, C.G., Baugh, C.M.& Frenk, C.S. 2000, MNRAS, 319, 168
Colin, J., Mohayaee, R., Sarkar, S., & Shafieloo, A. 2011, MNRAS, 414, 264
Croton, D. J., Springel, V., White, S. D. M., et al. 2006, MNRAS, 365, 11
Das, S., Mitra, S., Rotti, A., Pant, N., & Souradeep, T. 2014, arXiv:1401.7757
Dai, L., Jeong, D., Kamionkowski, M., & Chluba, J. 2013, Physical Review D, 87, 123005
De Lucia, G., & Blaizot, J. 2007, MNRAS, 375, 2

Eisenstein, D. J., Annis, J., Gunn, J. E., et al. 2001, AJ, 122, 2267
Fang, K., & Linden, T. 2015, Physical Review D, 91, 083501
Fixsen, D. J., Cheng, E. S., Gales, J. M., et al. 1996, ApJ, 473, 576
Gruppuso, A., Natoli, P., Paci, F., et al. 2013, JCAP, 7, 047
Gorski, K. M., Wandelt, B. D., Hansen, F. K., Hivon, E., & Banday, A. J. 1999, arXiv:astro-ph/9905275
Górski, K. M., Hivon, E., Banday, A. J., et al. 2005, ApJ, 622, 759
Gupta, S., & Saini, T. D. 2010, MNRAS, 407, 651
Guo, Q., White, S., Boylan-Kolchin, M., et al. 2011, MNRAS, 413, 101
Hajian, A., & Souradeep, T. 2003, ApJ Letters, 597, L5
Hamilton, A.J.S.ApJ, 385, L5
Hanson, D., & Lewis, A. 2009, Physical Review D, 80, 063004
Huterer, D., Shafer, D. L., & Schmidt, F. 2015, arXiv:1509.04708
Hazra, D. K., & Shafieloo, A. 2015, JCAP, 11, 012
Jackson, J. C. 2012, MNRAS, 426, 779
Javanmardi, B., Porciani, C., Kroupa, P., & Pflamm-Altenburg, J. 2015, ApJ, 810, 47
Kaiser, N. 1987, MNRAS, 227, 1
Kalus, B., Schwarz, D. J., Seikel, M., & Wiegand, A. 2013, A&A, 553, A56
Kang, X., Wang, P. 2015, ApJ, 813, 6
Kashlinsky, A., Atrio-Barandela, F., Kocevski, D., & Ebeling, H. 2008, ApJ Letters, 686, L49
Kashlinsky, A., Atrio-Barandela, F., Ebeling, H., Edge, A., & Kocevski, D. 2010, ApJ Letters, 712, L81
Kauffmann, G., White, S.D.M. & Guiderdoni, B. 1993, MNRAS, 264, 201
Kauffmann, G. & White, S.D.M. 1993, MNRAS, 261, 921
Kauffmann, G. 1996, MNRAS, 281, 487
Kolb, E. W., Matarrese, S., & Riotto, A. 2006, New Journal of Physics, 8, 322
Land, K., & Magueijo, J 2005, Physical Review Letters, 95, 071301
Lemson, G., & Virgo Consortium, t. 2006, arXiv:astro-ph/0608019
Lin, H.-N., Wang, S., Chang, Z., & Li, X. 2015, Accepted in MNRAS, arXiv:1504.03428
Marinoni, C., Bel, J., & Buzzi, A. 2012, JCAP, 10, 036
Marozzi, G., & Uzan, J.-P. 2012, Physical Review D, 86, 063528
Meegan, C. A., Fishman, G. J., Wilson, R. B., et al. 1992, Nature, 355, 143
Michalowicz, J.V., Nichols, J.M., Bucholtz, F. 2014, Handbook of differential entropy, CRC Press, Taylor & Francis Group, 2014
Moss, A., Scott, D., Zibin, J. P., & Battye, R. 2011, Physical Review D, 84, 023014
Mukherjee, S., Aluri, P. K., Das, S., Shaikh, S., & Souradeep, T. 2015, arXiv:1510.00154
Pandey, B. 2013, MNRAS, 430, 3376
Pandey, B., & Sarkar, S. 2015, MNRAS, 454, 2647
Pandey, B., & Sarkar, S. 2016, Accepted in MNRAS, arXiv:1512.06350
Penzias, A. A., & Wilson, R. W. 1965, ApJ, 142, 419
Pitrou, C., Pereira, T. S., & Uzan, J.-P. 2008, JCAP, 4, 004
Planck Collaboration, Ade, P. A. R., Aghanim, N., et al. 2014, A&A, 571, A23
Planck Collaboration, Ade, P. A. R., Aghanim, N., et al. 2015, arXiv:1506.07135
Schwarz, D. J., Starkman, G. D., Huterer, D., & Copi, C. J. 2004, Physical Review Letters, 93, 221301
Schwarz, D. J., & Weinhorst, B. 2007, A&A, 474, 717
Shannon, C. E. 1948, Bell System Technical Journal, 27, 379-423, 623-656
Scharf, C. A., Jahoda, K., Treyer, M., et al. 2000, ApJ, 544, 49
Shtanov, Y. 2010, Annalen der Physik, 522, 332
Smoot, G. F., Bennett, C. L., Kogut, A., et al. 1992, ApJ Letters, 396, L1
Soda, J. 2012, Classical and Quantum Gravity, 29, 083001
Somerville, R.S. & Primack, J.R. 1999, MNRAS, 310, 1087
Springel, V., White, S. D. M., Jenkins, A., et al. 2005, Nature, 435, 629
Taylor, S. R., & Gair, J. R. 2013, Physical Review D, 88, 084001
Watkins, R., Feldman, H. A., & Hudson, M. J. 2009, MNRAS, 392, 743
White, S. D. M. & Frenk, C. S. 1991, ApJ, 379, 52
Wilson, R. W., & Penzias, A. A. 1967, Science, 156, 1100
Wu, K. K. S., Lahav, O., & Rees, M. J. 1999, Nature, 397, 225
Zentner, A. R., Kravtsov, A. V., Gnedin, O. Y., & Klypin, A. A. 2005, ApJ, 629, 219
Zunckel, C., Huterer, D., & Starkman, G. D. 2011, Physical Review D, 84, 043005

This paper has been typeset from a TEX/LATEX file prepared by the author.